Published online March 29, 2018

Special Section: Lysimeters in Vadose Zone Research

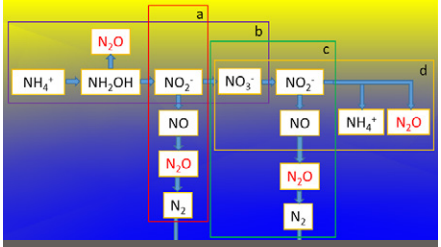

Core Ideas

- Dynamics of redox potential were induced by water-table changes in a lysimeter.
- The redox potential measurements well reflected the different GHG emission sources.
- Redox potential monitoring is a viable tool for better understanding of GHG emissions.

Agrosphere Institute (IBG-3), Forschungszentrum Jülich, Jülich 52425, Germany. *Corresponding author (ji.wang@fz-juelich.de).

Received 18 Aug. 2017.
Accepted 19 Dec. 2017.

Citation: Wang, J., H.R. Bogena, H. Vereecken, and N. Brüggemann. 2018. Characterizing redox potential effects on greenhouse gas emissions induced by water-level changes. Vadose Zone J. 17:170152. doi:10.2136/vzj2017.08.0152

Characterizing Redox Potential Effects on Greenhouse Gas Emissions Induced by Water-Level Changes

Jihuan Wang,* Heye R. Bogena, Harry Vereecken, and Nicolas Brüggemann

Soil greenhouse gas (GHG) emissions contribute to global warming. To support mitigation measures against global warming, it is important to understand the controlling processes of GHG emissions. Previous studies focusing mainly on paddy rice fields or wetlands showed a strong relationship between soil redox potential and GHG emission (e.g., N_2O). However, the interpretation of redox potentials for the understanding of the controlling factors of GHG emission is limited due to the low number of continuous redox measurements in most ecosystems. Recent sensor developments open the possibility for the long-term monitoring of field-scale soil redox potential changes. We performed laboratory lysimeter experiments to investigate how changes in the redox potential, induced by changes in the water level, affect GHG emissions from agricultural soil. Under our experimental conditions, we found that N_2O emissions followed closely the changes in redox potential. The dynamics of redox potential were induced by changing the water-table depth in a laboratory lysimeter. Before fertilization during saturated conditions, we found a clear negative correlation between redox potentials and N_2O emission rates. After switching from saturated to unsaturated conditions, N_2O emission quickly decreased, indicating denitrification as the main source of N_2O. In contrast, the emissions of CO_2 increased with increasing soil redox potentials. After fertilization, N_2O emission peaked at high redox potential, suggesting nitrification as the main production pathway, which was confirmed by isotope analysis of N_2O. We propose that redox potential measurements are a viable method for better understanding of the controlling factors of GHG emissions, for the differentiation between different source processes, and for the improvement of process-based GHG models.

Abbreviations: GHG, greenhouse gas; SP, site preference.

The greenhouse gases CO_2, CH_4, and N_2O are recognized as the most important contributors to global warming. Large amounts of C and N are stored in the top soil layer (1 m) of the Earth, accounting for about 1500 Pg C (Batjes, 1996; Bruce et al., 1999; Johnson and Henderson, 1995) and an estimated 133 to 140 Pg N (Batjes, 1996; Post et al., 1985). Thus, soil comprises the largest terrestrial C and N pools (Kutsch et al., 2009; Nieder and Benbi, 2008; Schaufler et al., 2010; Schlesinger and Andrews, 2000). According to the Intergovernmental Panel on Climate Change, total GHG emissions in agriculture, forestry, and other land uses (e.g., cropland, grassland, and biomass burning) contribute about 25% of global GHG emissions using 100-yr global warming potential metrics (Pachauri et al., 2014). Furthermore, agricultural N_2O emissions contributed about 60% of total anthropogenic N_2O emissions in 2005 (Reay et al., 2012) and amounted to 4% of global GHG emissions in 2010 (Olivier and Janssens-Maenhout, 2012). Therefore, the study of biogeochemical processes in soils is critical to better understand the controlling factors of soil GHG fluxes and to more effectively reduce soil GHG emissions.

Many studies have investigated GHG emissions from soils under natural conditions (Dalal et al., 2003; Le Mer and Roger, 2001; Martikainen et al., 1993; Moore and Knowles, 1989; Šimůnek and Suarez, 1993; Weihermüller et al., 2009) or under controlled soil temperature and soil moisture conditions (del Prado et al., 2006; Ruser et al., 2006; Schaufler et

al., 2010) but usually without measurements of soil redox conditions (Eh). Under field conditions, soil moisture and temperature are covaried or interact, which may complicate the discrimination of the controlling mechanisms of GHG emission (Fang and Moncrieff, 2001).

Although redox potential measurements have shown to be useful to better understand the hydrological control on biogeochemical processes that govern GHG emissions (Rubol et al., 2012), few studies have focused on the effects of soil redox conditions on soil GHG emissions. Flessa and Beese (1995) showed that N_2O emissions increased after application of N in the form of sugar beet residues during low redox potential conditions, and Yu and Patrick (2003) found higher emission rates of N_2O and CH_4 during moderately reducing to reducing conditions for paddy soils. Nitrous oxide can be produced by nitrification at high redox potentials (400 mV) or by denitrification processes in O_2–deficient environments (200 mV and lower), whereas CH_4 emissions typically occur under extended anaerobic conditions (–150 mV and lower) (Masscheleyn et al., 1993). Rezanezhad et al. (2014) performed laboratory column experiments with fluctuating water tables and showed that induced redox potential changes between –100 and 700 mV affected CO_2 emission as well as the distribution of nutrients. The above studies indicated that the different controlling factors of GHG emissions are interrelated in a complex way and that more information on the interplay of O_2 availability, redox potential, and GHG emission is needed to improve the accuracy of GHG emission models (Rubol et al., 2012).

In environmental science, the redox potential is often used as a criterion for the oxidation–reduction status of water bodies, sediments, and soils (Fiedler et al., 2007) that governs the production and consumption of GHG (Yu and Patrick, 2003). For instance, frequent fluctuations of soil water content may favor N_2O production and its emission to the atmosphere because N_2O efflux was found to be greatest at moderately reducing conditions (Smith et al., 2003). In this respect, oxidation is defined as removal of electrons from a chemical compound, and reduction is defined as the uptake of electrons by a chemical compound (Bhaumik and Clark, 1948; Delaune and Reddy, 2005). A high redox potential favors the oxidation of reduced compounds, whereas a low redox potential promotes reduction of oxidized compounds.

The soil microbial community is highly sensitive to soil aeration conditions. In the case of a sufficient O_2 concentration, the aerobic microorganism populations thrive, whereas the activity of anaerobic microorganisms is suppressed (Porter et al., 2004). The decline of redox potential during conditions of insufficient supply of O_2 is caused by microbial consumption of O_2. This decreasing trend in redox potential indicates that certain populations of microbes continue to utilize the free energy from easily decomposable organic compounds despite the reduced O_2 availability. Because this situation is variable in the soil due to the nonuniform distribution of organic material, the redox potential also shows a high spatial variability (Fiedler et al., 2007; Mansfeldt, 2004).

The main microbial processes controlling the redox status in soils are (i) redox processes in which inorganic substances are used as electron acceptors (O_2, NO_3^-, NO_2^-, NO, N_2O, oxidized Mn compounds, ferric oxides, sulfate, CO_2) and (ii) fermentative processes in which organic molecules are used as electron donors (Delaune and Reddy, 2005). Under O_2–rich conditions, the organic sources are the most important sources for redox reactions (Pezeshki and DeLaune, 2012). The abundance and activity of oxidized and reduced chemical substances cause specific electrochemical potentials that can be measured as a potential difference between an inert indicator electrode and a reference electrode using a voltmeter (Delaune and Reddy, 2005; Farrell et al., 1991; Fiedler et al., 2007; Flessa and Beese, 1995; Mansfeldt, 2004; Wang et al., 1993; Yu et al., 2001). The soil redox potential typically follows quickly the changes in O_2 availability in the soil (Fiedler et al., 2007). In addition, redox potential measurements are relatively inexpensive and easy to maintain and thus are suitable for laboratory as well as field applications for the long-term measurements of redox conditions in soil.

Figure 1 shows the interrelation between GHG emissions, N-cycle processes, saturation status, and redox potential. This study aimed for a better understanding of the relationship between soil water content, soil water potential, redox potentials, and the biogeochemical soil processes related to GHG emissions using a set of continuously monitored long-term laboratory column experiments with controlled water levels. The specific objectives of the study were (i) to identify soil Eh characteristics under different soil saturation conditions with in situ redox measurements in laboratory experiments with a lysimeter setup, (ii) to investigate the relationship between redox potential changes and N_2O and

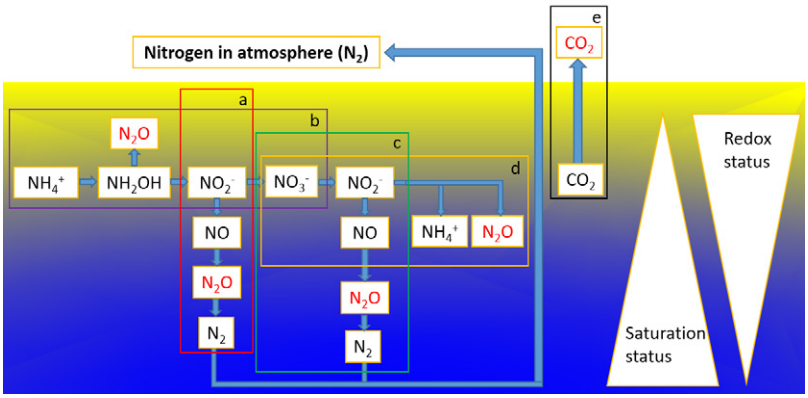

Fig. 1. Interrelation between greenhouse gas emissions, N-cycle processes, saturation status, and redox status: nitrifier denitrification (a), nitrification (b), denitrification (c), nitrite ammonification (d), and respiration (e).

CO_2 emissions, and (iii) to discuss the potential of in situ redox measurements for the investigation of the controlling processes of GHG emission.

Materials and Methods

Soil Samples

The soil material used for the lysimeter experiments originated from the TERENO agricultural test site Selhausen, which is part of the TERENO observatory Eifel/Lower Rhine Valley (Bogena et al., 2012). The Selhausen site is a 9.6-ha agricultural field located in the lower Rhine valley in western Germany, a heterogeneous rural agricultural area that belongs to the temperate maritime climate zone (Korres et al., 2015). The mean annual temperature and precipitation from 1961 to 2014 were about 10°C and 714 mm, respectively. The main soil type is Haplic Luvisol with a silt loam texture. On 17 Jan. 2016, 30 samples from the Ap horizon (0–30-cm depth) were taken at 15 different points evenly distributed across the field to capture the local soil variability. The soil material was mixed, air dried, sieved to particle sizes <2 mm, and analyzed for important soil physical and chemical properties in the laboratory. The amount of soil particles >2 mm was negligible. The main characteristics of the soil material are shown in Table 1.

Table 1. Main characteristics of the soil material used for the lysimeter experiment.

Parameter	Value
Soil texture, %	
Clay	17.8
Fine silt	7.5
Medium silt	19.7
Coarse silt	41.2
Sand	13.8
Soil characteristics	
Organic C, %	1.12 ± 0.01
Total N, %	0.14 ± 0.01
pH	7.3 ± 0.1
NH_4^+, mg kg^{-1} SDW†	46.42 ± 5
NO_3^-, mg kg^{-1} SDW	4.25 ± 0.4

† SDW, soil dry weight.

Experimental Design

For the experiments on the effect of varying water table depth and fertilization on soil GHG fluxes, a laboratory lysimeter (EcoTech; schematic setup shown in Fig. 2) was used (height, 50 cm; diameter, 30 cm) as the container for the soil column. The soil column height was ~47 cm. The lower boundary of the lysimeter was a porous nylon membrane plate with an air-entry pressure of 0.2 MPa. The lysimeter was carefully filled with ~42.7 kg of dried Selhausen soil material. The soil was compacted every 8 cm to achieve a homogenous bulk density corresponding to the bulk density of the soil in the field (1.26 g cm^{-3}). During the experiment, the soil column was partially saturated with tap water, and the water table inside the lysimeter was controlled using a Mariotte bottle and monitored with a transparent tube connected to the line between the Mariotte bottle and the lysimeter (Fig. 2). The depth of the capillary in the Mariotte bottle defined the level of atmospheric pressure and thus the water table in the soil column. A gas chamber was placed air-tight on top of the lysimeter at regular intervals for GHG measurements. A small membrane inset in the gas chamber enabled gas sampling with a syringe. Redox potentials were measured using a system of redox and reference electrodes according to Mansfeldt (2004) (described below). Three platinum electrodes were installed 3, 11, and 19 cm below the soil surface, and a reference electrode with an Ag–AgCl salt bridge was inserted vertically into a 15-cm-deep borehole in the center of the lysimeter following Weigand et al. (2010). To secure a proper contact between the soil and salt bridge, the hole was filled with slurry from the soil material. The soil water potential was measured at depths of 3, 11, 19, and 35 cm with eight laboratory tensiometers (T5, Meter Group AG).

To check whether the tensiometers provided reliable data, we compared the tensiometer data with the measured water levels (i.e., the positive pressure values should correspond to the water column above the tensiometer). We corrected deviations between the water table and pressure heights by calculating the respective offset values for each tensiometer (Fig. 3). Stronger deviations

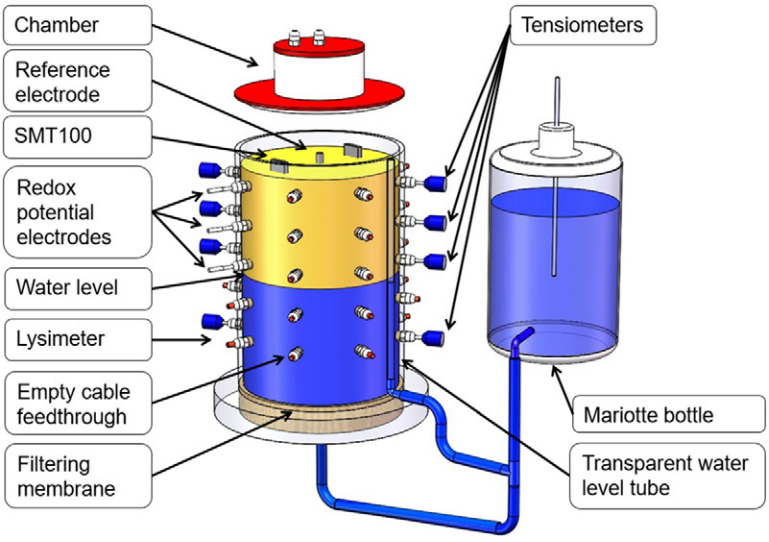

Fig. 2. Schematic diagram of the lysimeter system used for the experiments. A Mariotte bottle was used to control the water table height in the lysimeter, and the closed chamber method was used to measure the fluxes of greenhouse gases (PT100 sensors are not shown).

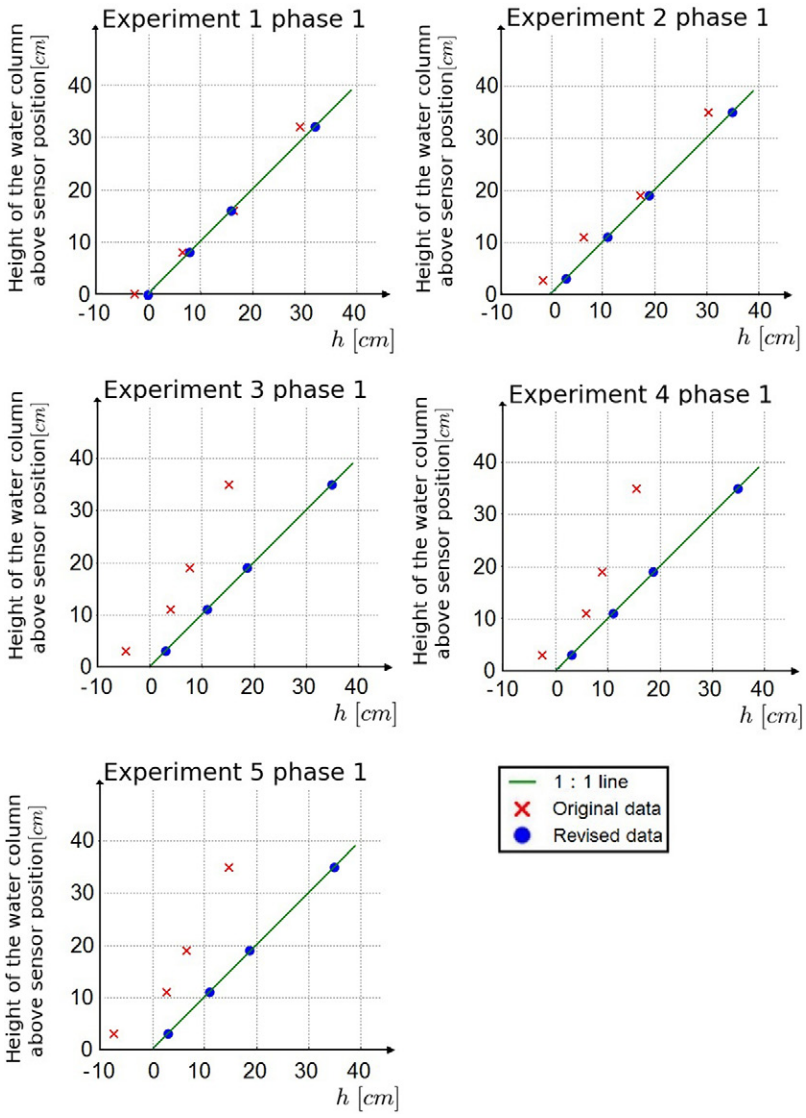

Fig. 3. Measured water potential (h) vs. the corresponding water depth above the sensor (z) averaged under quasi-equilibrium conditions (after ~3 d) before and after offset correction by taking the mean value of tensiometers at four different depths. Phase 1 indicates the period with the highest water table level.

occurred after a longer period of unsaturated soil conditions between Exp. 2 and 3, possibly due to air intrusion into the porous cups of the tensiometers.

Two PT100 temperature sensors and two soil moisture sensors were installed at two different depths (SMT100, Truebner GmbH). All measured data were continuously logged every minute with a DataTaker DT 85 datalogger (Thermo Fisher Scientific).

Multistep Groundwater Level Experiments

In our lysimeter experiments, different soil saturation and redox potential states were induced by controlling the groundwater table in the lysimeter by means of the Mariotte bottle as shown in Fig. 2. In total, five multistep groundwater level experiments were performed at a constant temperature of ~18°C. Before the first experiment, the soil was well drained from 22 May to 3 June. At each step, the water table was kept stable for about 1 wk, and gas samples were taken once or twice every day. The five experiments can be divided into two parts (i.e., two experiments before and three experiments after the onset of fertilization). Each experiment took about 1 mo, during which time the water table level, soil water potential, and redox potentials were continuously monitored. At the beginning of each experiment, the soil was fully saturated by setting the water table to the level of the soil surface (Fig. 4a and 5a). In the first experiment, the water table did not fully reach the soil surface because of a missing water table level control, which was installed before the second experiment to improve the leveling of the water table (Fig. 2). Subsequently, the water table was lowered in a multistep fashion in which the water table was kept stable for about 7 d and then decreased by about 8 cm each time. About 2 d after changing the level of the tube in the Mariotte bottle, the water table inside the lysimeter had returned to equilibrium with the pressure level of the Mariotte bottle.

The first and the second experiments were performed with original field soil without additional fertilization. After Exp. 2 was complete, the soil in the lysimeter was fertilized with 1.6 g calcium ammonium nitrate (13.5% NO_3^-–N, 13.5% NH_4^+–N, corresponding to 60 kg N ha^{-1}) dissolved in 5.2 L of tap water in the Mariotte bottle. We introduced the fertilizer in dissolved form via the Mariotte bottle to achieve a virtually homogeneous distribution throughout the soil column.

At the end of the experiments, ~2 g of soil material was sampled from the soil column at depths of 3, 11, 19, 27, and 35 cm. Each soil sample was extracted using 50 mL of 0.1 M $CaCl_2$ solution. The concentrations of NH_4^+ and NO_3^- in the extracted soil solution were analyzed using a Dionex ICS-3000.

The air temperature in the experiments ranged from 16.6 to 22.5°C (mean, 18.0°C; SD, 0.9°C) (data not shown). The mean temperature in the soil was 18.0°C at the 11-cm depth (SD, 0.8°C) and 19.0°C at the 35-cm depth (SD, 0.7°C), indicating increasing soil temperature with depth (data not shown). Given these low variations in temperature, we assumed that changes in soil temperature were not a critical factor for CO_2 and N_2O formation and emission in our experiments. We found that the soil CO_2 and N_2O fluxes could be better described with variations in soil water potential and water table depths than with soil temperature changes, which can be explained by the low temperature range of 5.9°C in our experiments (Schaufler et al., 2010).

Greenhouse Gas Flux Measurements

A long (1.5 m) and thin (diameter, 0.2 cm) tube was used to connect the chamber (diameter, 20 cm; height, 18 cm; volume, 5.65 L) with the ambient air as a vent tube to keep the inner air pressure equal to the ambient atmospheric pressure. Gas samples were taken every day throughout most of the experimental periods. Before the air samples were taken, the chamber was connected gas-tight with the soil column to avoid contamination with ambient air. The gas samples (40 mL each) were taken every 10 min during a 40-min period with a gas-tight syringe. The first sample was taken directly after closing the chamber to determine the GHG concentration of the ambient air (i.e., each flux measurement consisted of five samples). Each sample was transferred to a pre-evacuated glass vial (22 mL each), creating overpressure, and GHG concentrations were analyzed within 20 d after sampling with a gas chromatograph (Model 8610C, SRI). For flux calculations, a linear regression of the concentration–time correlation for each set of five samples of one gas flux measurement was performed. Parkin and Venterea (2010) provided a thorough discussion of uncertainties in the gas flux calculation. The slope of the respective regression equations was used to calculate CO_2 and N_2O fluxes:

$$F = \frac{bV_{Ch}MW \times 10^6}{A_{Ch}MV_{Corr} \times 10^9} \quad [1]$$

where F is the flux rate of CO_2 (mg C m^{-2} h^{-1}) or N_2O (μg N m^{-2} h^{-1}); b is the measured increase in CO_2–C or N_2O–N in the chamber (slope of the linear regression) (μL L^{-1} h^{-1} or

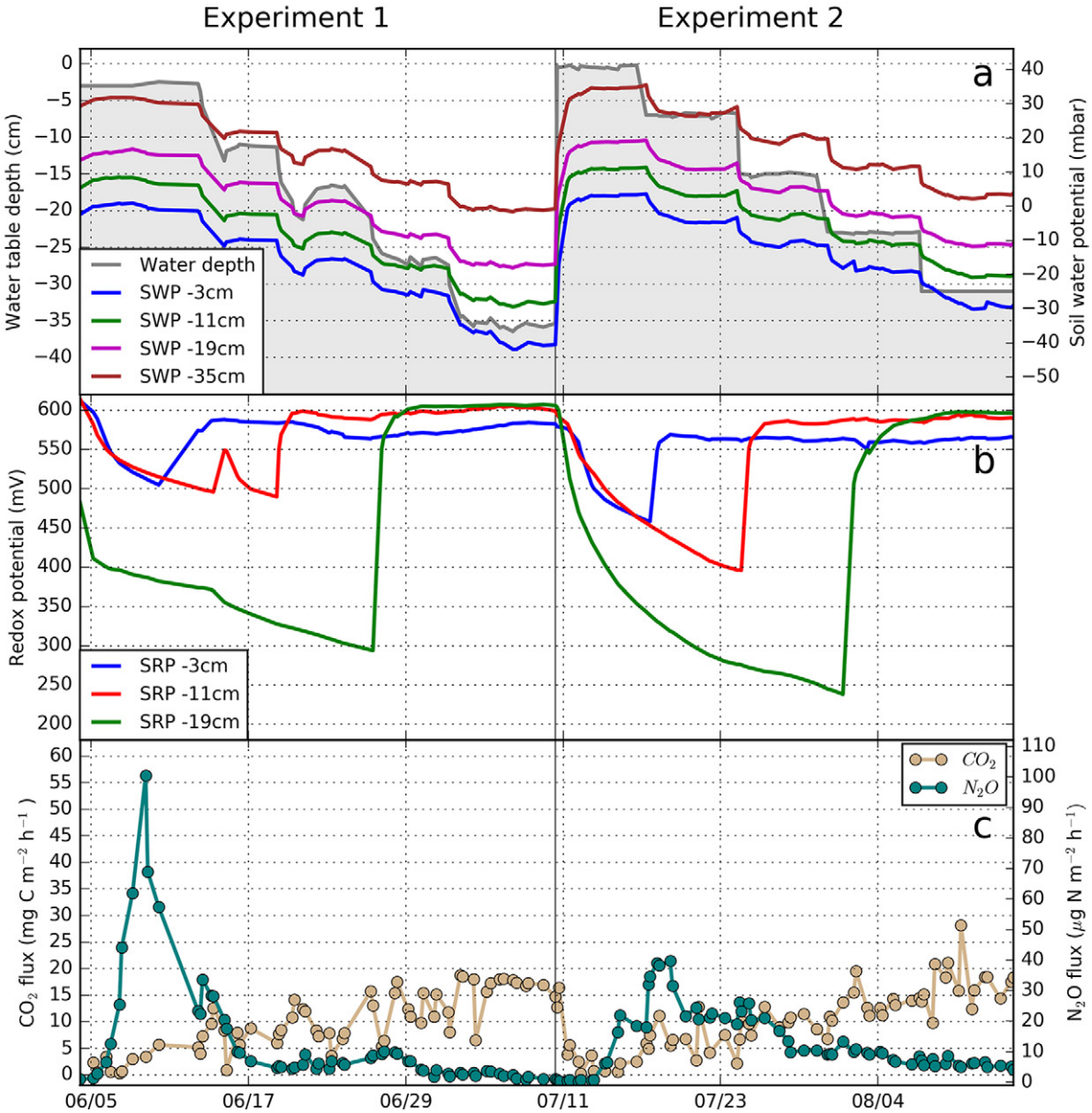

Fig. 4. Changes in water table, soil water potential (SWP; 1 mbar = 0.1 kPa), soil redox potential (SRP), and CO_2 and N_2O emission rates during Exp. 1 and 2 (before fertilizer application).

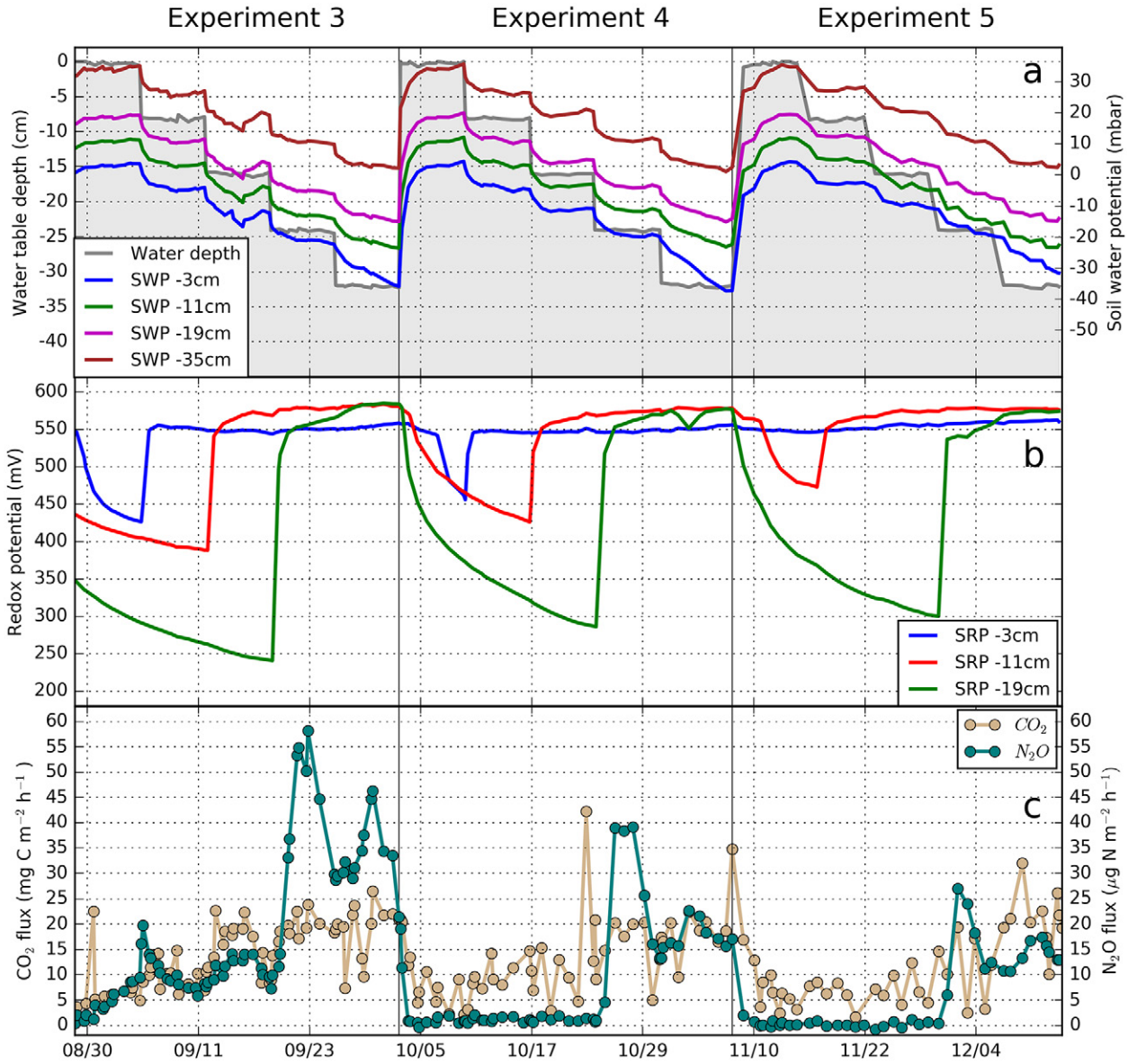

Fig. 5. Changes in water table, soil water potential (SWP; 1 mbar = 0.1 kPa), soil redox potential (SRP), and CO_2 and N_2O emission rates during Exp. 3, 4, and 5 (after fertilizer application).

nL L^{-1} h^{-1}); MW is the molecular weight of CO_2–C or N_2O–N; A_{Ch} (m^2) and V_{Ch} (m^3) are the base area and volume of the chamber, respectively; and MV_{Corr} is the pressure- and temperature-corrected molar volume of air (m^3 mol^{-1}), which was calculated using

$$MV_{Corr} = 0.02241 \left(\frac{273.15+t}{273.15}\right)\left(\frac{p_0}{p_1}\right) \quad [2]$$

where t is the air temperature during measurements (°C), p_0 is the standard atmospheric air pressure (Pa), and p_1 is the air pressure during measurements (Pa) (Brümmer et al., 2008; Collier et al., 2014). The mean R^2 values of the linear correlations for the CO_2 and N_2O flux calculations were 0.92 and 0.97, respectively. Flux values were accepted when the R^2 value of the linear regression was >0.8 or assumed to be zero when the deviation of the concentration values of the five different time points from the mean of the five samples was <2 SD. Negative CO_2 fluxes, which occurred when the initial CO_2 background in the chamber headspace was higher than normal, leading to a CO_2 flux into the soil column, were omitted.

Identification of Nitrous Oxide Source Processes

To identify the source processes of N_2O in Exp. 5, additional gas samples were taken for the isotopic signature analysis of N_2O ($\delta^{15}N$, $\delta^{18}O$, and ^{15}N site preference [SP]). The SP is defined as the difference between $\delta^{15}N^{\alpha}$ (central N) and $\delta^{15}N^{\beta}$ (terminal N) in the asymmetric N_2O molecule. Decock and Six (2013) classified the average SP values (±SD) for N_2O from denitrification

and nitrifier denitrification as −1.6 ± 3.8‰ and as 32.8 ± 4.0‰ from NH_3 or hydroxylamine oxidation by NH_3–oxidizing bacteria and archaea, fungal denitrification, and abiotic hydroxylamine oxidation.

Immediately after the end of each GHG measurement in Exp. 5 (i.e., after a 40-min closure time), a 125-mL gas sample was taken from the chamber that was still placed on top of the soil column and transferred to a 120-mL serum bottle that had been crimped to be gas tight with an aluminum cap and a butyl rubber septum and pre-evacuated before use. Subsequently, the $\delta^{15}N_{bulk}$, $\delta^{18}O$, and SP of N_2O were analyzed using an isotope-ratio mass spectrometer (IsoPrime 100, Elementar Analysensysteme). For details of the analysis, see Heil et al. (2015). The SP and $\delta^{18}O$ values of N_2O source were calculated according to the binary mixing model of Wei et al. (2017), correcting for the N_2O background of the ambient air:

$$SP_s = \frac{SP_m C_m - SP_a C_a}{C_m - C_a} \quad [3]$$

where SP_s, SP_m, and SP_a are the SP values of N_2O from soil, the mixture of N_2O from soil and ambient air in the vial headspace, and N_2O in the ambient air, respectively; and C_m and C_a are the N_2O concentrations in the vial headspace and ambient air, respectively.

Redox Potential Measurements

The relative proportions of oxidized and reduced substances in the soil determine the redox status of the soil, which can be expressed as redox potential in volts or millivolts by the Nernst equation (Mitsch and Gosselink, 2007):

$$Eh = E_0 + 2.3\frac{RT}{nF}\log_e\frac{A}{B} \quad [4]$$

where A and B are the concentrations of oxidized and reduced compounds, respectively; E_0 is the standard half-cell potential; R is the universal gas constant; T is the absolute temperature; F is the Faraday constant; and n is the number of electrons exchanged. The higher the proportion of oxidized to reduced compounds, the higher Eh, and vice versa. The redox potential can be measured using a reference electrode (e.g., Ag–AgCl) and a working electrode (e.g., Pt). The redox potential measurements are related to the normal hydrogen electrode using

$$Eh = E + E_{ref} \quad [5]$$

in which E is the potential measured against the Ag–AgCl reference electrode, and E_{ref} is the voltage difference between the standard hydrogen reference electrode and the Ag–AgCl reference electrode (210.5 mV at 20°C) (Fiedler et al., 2007).

Statistical Analysis

Statistical analyses were conducted with the Python package, version 3.6, using the Pandas and NumPy libraries. Regression analysis was performed to identify the optimal regression function based on the maximum R^2 value for the relationship between the water potential at the respective depth and CO_2 and N_2O emissions before and after fertilization (Table 2).

Results and Discussion

Soil Redox Potential

During each phase of saturated conditions, the redox potential started to decrease in each of the three depths, indicating O_2 consumption by soil microbial activity (Fig. 4b). However, the redox potential in the upper part of the soil column declined more slowly than the redox potential in the lower part of the lysimeter, where

Table 2. Functional relationships between soil water potential and CO_2 and N_2O emissions (ψ, soil water potential in mbar [1 mbar = 0.1 kPa]; F_{CO2}, CO_2 emission rate in mg C m^{-2} h^{-1}; F_{N2O}, N_2O emission rate in μg N m^{-2} h^{-1}).

	Linear regression			Linear or exponential regression		
Depth	Equation	R^2	*P* value	Equation	R^2	*P* value
cm						
Before fertilization (Exp. 1 and 2)						
3	$F_{CO2} = -0.3647\psi + 4.481$	0.6543	<0.001	$F_{N2O} = 61.84\exp[0.10(\psi - 5.55)] + 2.54$	0.4641	<0.001
11	$F_{CO2} = -0.3878\psi + 7.28$	0.6526	<0.001	$F_{N2O} = 81.84\exp[0.10(\psi - 16.19)] + 2.28$	0.4553	<0.001
19	$F_{CO2} = -0.4168\psi + 10.70$	0.6660	<0.001	$F_{N2O} = 87.27\exp[0.07(\psi - 31.37)] - 0.11$	0.4536	<0.001
35	$F_{CO2} = -0.4195\psi + 16.99$	0.6883	<0.001	$F_{N2O} = 78.84\exp[0.14(\psi - 36.45)] + 4.07$	0.5002	0.332
After fertilization (Exp. 3–5)						
3	$F_{CO2} = -0.4237\psi + 7.86$	0.4682	<0.001	$F_{N2O} = -0.7614\psi + 2.697$	0.4514	<0.001
11	$F_{CO2} = -0.4326\psi + 11.19$	0.4462	<0.001	$F_{N2O} = -0.7871\psi + 8.639$	0.4418	<0.001
19	$F_{CO2} = -0.4366\psi + 14.58$	0.4449	<0.001	$F_{N2O} = -0.7967\psi + 14.82$	0.4432	<0.001
35	$F_{CO2} = -0.4404\psi + 21.47$	0.4379	<0.001	$F_{N2O} = -0.8087\psi + 27.48$	0.4420	<0.001

O_2 was more rapidly consumed as indicated by the fast decline in redox potential. The total range of the redox potential differed greatly among the three depths (from 450 to 600 mV at −3 cm and from 250 to 600 mV at −19 cm). During the following three experiments after adding fertilizer to the water reservoir of the Mariotte bottle, the water table was controlled in the same fashion as in the first two experiments, producing very similar responses in soil water potential (Fig. 4a) and redox potential (Fig. 4b).

Carbon Dioxide Emissions

The soil water potential measurements (average of two sensors per depth) showed close correlation with water table changes at each level, indicating that soil water drainage was not hindered during the experiments (Fig. 4a). Because the water potential changes were virtually identical at the different depths, we compared CO_2 fluxes only with the water potential at the 3-cm depth. We found a positive correlation between soil water potential and CO_2 fluxes in unfertilized soil (R^2 = 0.65) and in fertilized soil (R^2 = 0.47) (Fig. 6; Table 2). The slope of the linear regression equation of CO_2 emission vs. water potential ranged between −0.42 and −0.36 before fertilization (Table 2). After fertilization, the slope increased to values between −0.44 and −0.42. The R^2 was substantially lower for the experiments after fertilization. Carbon dioxide emissions showed a similar response to changes in soil water potential as during the earlier experiments and thus seemed not to be strongly influenced by the fertilization event (Fig. 5c).

Under saturated conditions, CO_2 fluxes were very low (range, 3–5 mg C m^{-2} h^{-1}). With decreasing water levels, CO_2 emissions increased gradually, reaching maximum values of 20 to 25 mg C m^{-2} h^{-1} as the water table reached −31 cm (Fig. 4c). The mean CO_2 emission rates in Exp. 1 to 5 were 223.0, 242.3, 323.9, 298.4, and 263.5 mg CO_2–C m^{-2} d^{-1}, respectively. The variations in water table and soil water potential were primarily responsible for the observed variations in CO_2 emissions through their influence on O_2 availability and respiration by soil microorganisms (Hou et al., 2000; Oertel et al., 2016; Sainju et al., 2006; Weihermüller et al., 2009). In addition, as water content decreases, the water–gas interfacial area enlarges due to the increase in soil air content, leading to enhanced gaseous diffusion and exchange with the atmosphere (Oertel et al., 2016). It is very likely that this effect contributed to the enhanced CO_2 emission rates under lower saturation conditions in our experiments. Because there were no CO_2 and N_2O emissions determined during the onset of the fertilization event, this period is not shown in Fig. 4 and 5.

Nitrous Oxide Emissions

Before fertilization and a few days after saturation of the soil column, an initial peak of N_2O emission of about 100 μg N_2O–N m^{-2} h^{-1} was observed in Exp. 1. This was followed by a fast decrease (Fig. 4c), which is consistent with an initial NO_3^- pool being quickly depleted via denitrification. With each step of lowering the water table in Exp. 1, the N_2O emission rate slightly increased but then started to decrease again. The highest N_2O emission rate during Exp. 1 went along with the lowest redox potential at the 3-cm depth and was about 2.5 times as high as the highest N_2O emission during Exp. 2 (~100 μg N m^{-2} h^{-1} compared with <40 μg N m^{-2} h^{-1}) (Fig. 4c), which might be the result of progressive consumption of N substrate (NO_3^-) in the soil (note that no N was added in the first two experiments). In Exp. 2, the highest N_2O emission rate occurred when the redox potential at the 3-cm depth was minimal. Figure 4c also reveals a time lag of the emission peaks of N_2O after the redox potential changes. The N_2O emission was more strongly affected by the fertilizer treatment (Fig. 5c). In contrast to the first two experiments before fertilization, where N_2O emissions peaked at decreasing redox potential, N_2O emissions after fertilization occurred immediately after the redox potential at the lowest depth (19 cm) increased after the water table decreased below this depth (Fig. 5a–5c). In addition, peak N_2O emission rates decreased from Exp. 3 to Exp. 5

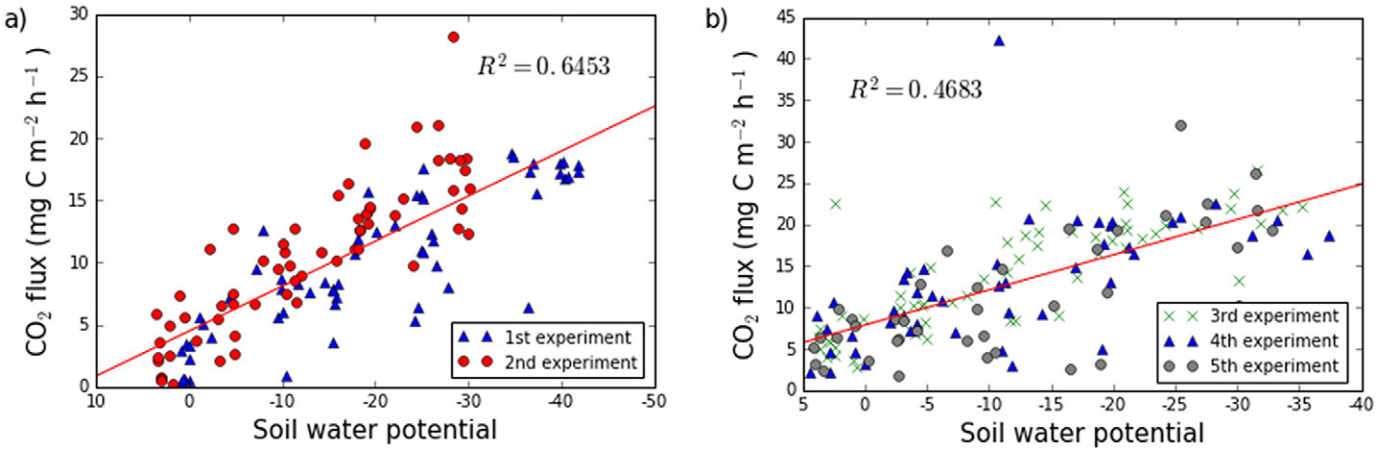

Fig. 6. Carbon dioxide emissions vs. the soil water potential (in mbar; 1 mbar = 0.1 kPa) measured at 3 cm below the soil surface (a) without and (b) with fertilization application. The corresponding regression equations are given in Table 2.

(from ~60 to <30 μg N m^{-2} h^{-1}) but were much lower than the emission peak in Exp. 1 (~100 μg N m^{-2} h^{-1}). However, the N_2O emission peak in Exp. 3 (60 μg N m^{-2} h^{-1}) was higher than the peak in Exp. 2 (40 μg N m^{-2} h^{-1}). The mean N_2O emission rates in Exp. 1 to 5 were 341.9, 310.8, 459.8, 224.7, and 137.5 μg N_2O–N m^{-2} d^{-1}, respectively.

Figure 7a shows an exponential relationship between N_2O emissions and water potential changes, where most of the large N_2O emissions occurred at lower redox potential (wet conditions) before fertilization. This effect can be explained by the strong depletion of O_2 in the soil column, promoting anoxic microsites, which foster N_2O emissions by denitrification (Flessa and Beese, 1995). In contrast, a positive linear correlation between soil water potential and N_2O production was found after fertilization (Fig. 7b), which points to nitrification as the main source of N_2O at lower water potentials, which primarily occur at higher redox potentials. Thus, the determination of the relationship between N_2O emission and soil water potential at different depths could be useful for quantifying the relative contribution of the different source processes of N_2O in the soil (i.e., nitrification and denitrification).

The peak N_2O emissions in Exp. 1 and 2 occurred with a time lag of about 3 d after complete saturation of the soil. Even though this change in water regime restricted the O_2 availability in the soil, there might have been some residual air stored in the air-filled pore space (Gardner et al., 1999), which might have retarded the onset of denitrification. However, when the soil is waterlogged for a longer time, the N_2O is reduced to N_2, which also can explain the decrease in N_2O emissions after the N_2O peaks in Exp. 1 and 2. A further explanation for the decrease in N_2O emissions might be the depletion of available substrate, mainly NO_3^-.

Figure 8 shows the redox potential at three different depths and the CO_2 emissions before (Fig. 8a) and after (Fig. 8b) fertilization. Figure 9 shows the redox potential at three different depths and the N_2O emissions before (Fig. 9a) and after (Fig. 9b) fertilization. Compared with the fertilized soil, the release of N_2O in the unfertilized soil mainly occurred when the soil redox potential was lower. The highest N_2O emissions occurred when the redox potential at a depth of 19 cm ranged between 350 and 400 mV and when the values below the 19-cm depth should have been <350 mV. In incubation experiments with paddy soils, Yu et al. (2007) observed significant N_2O production between 200 and 500 mV and noted that nitrification could have contributed to N_2O production at Eh values >500 mV under well-aerated conditions (Tokarz and Urban, 2015). Furthermore, Brettar et al. (2002) suggested that an even lower range of redox potentials (10–300 mV) indicated denitrification in forest soils. Therefore, in our experiments without fertilization (Fig. 9a), denitrification was probably the source of N_2O emissions. In contrast, Fig. 9b indicates that nitrification was the dominant source of N_2O after the soil had been fertilized, although smaller N_2O emission peaks also occurred at lower redox potentials, possibly due to denitrification.

Figure 10 shows that the concentration of NO_3^- in the soil had decreased with soil depth at the end of Exp. 5. This may be a result of denitrification that used NO_3^- as a substrate under anaerobic conditions because saturated and thus anaerobic conditions lasted much longer with increasing soil depth. Accordingly, more NO_3^- was consumed in the lower part of the soil column but without detectable N_2O release at the surface, which was probably due to full N_2O reduction to N_2O under the strictly anaerobic conditions in the lower part of the soil column during most of the experiments. Because the fertilizer solution was added to the soil from the bottom of the lysimeter and because the mobility of NH_4^+ is relatively low, NH_4^+ accumulated in the lower part of the soil column. In addition, the consumption of NH_4^+ through nitrification under aerobic conditions reduced the NH_4^+ content in the upper part of the soil column and led to NO_3^- concentrations above the level of the original soil.

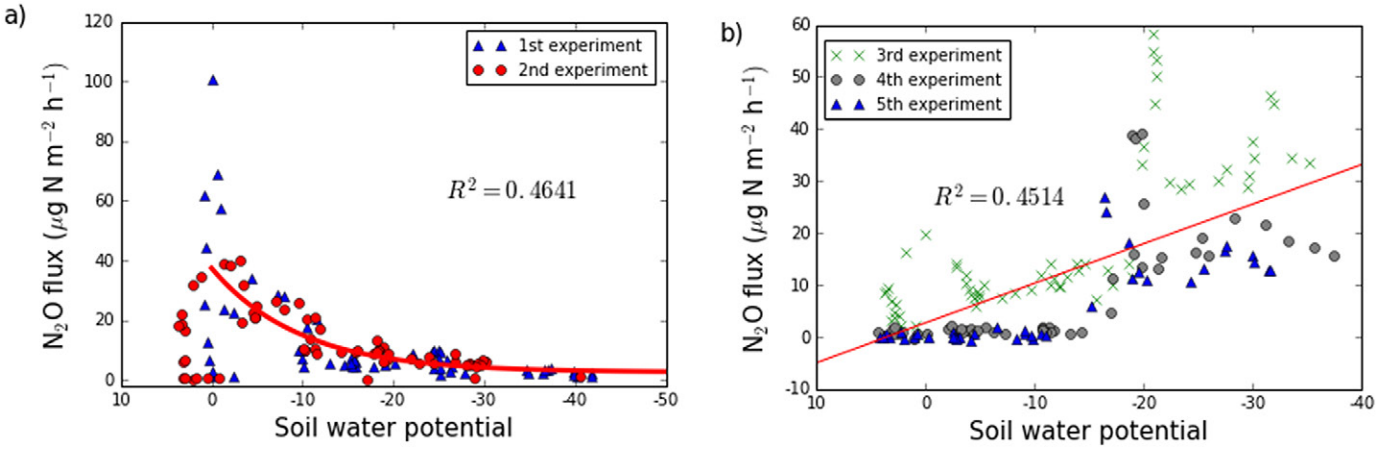

Fig. 7. Nitrous oxide emissions vs. the soil water potential (in mbar; 1 mbar = 0.1 kPa) measured at 3 cm below the soil surface (a) without and (b) with fertilization application. The corresponding regression equations are given in Table 2.

Nitrous oxide emission from the soil is facilitated via different interrelated processes (Butterbach-Bahl et al., 2013; Lewicka-Szczebak et al., 2017). The interpretation of the relations from the particular isotopic signatures in N_2O can be facilitated by an end-member analysis. End-member maps of ^{15}N SP and the $\delta^{18}O$ signatures of N_2O emitted are used to identify the sources of N_2O (Lewicka-Szczebak et al., 2017; Toyoda et al., 2015; Wei et al., 2017). The ranges of SP and $\delta^{18}O$ values were defined as 27 to 37 and 40 to 50‰, respectively, for nitrification (Sutka et al., 2006); 34 to 40 and 30 to 40‰, respectively, for fungal denitrification (Sutka et al., 2008; Wu et al., 2017); and −11 to 1.4 and 10 to 20‰, respectively, for bacterial denitrification (Toyoda et al., 2005; Wei et al., 2017; Zou et al., 2014). The specific SP–$\delta^{18}O$ relationship ranges for the different N_2O production processes are symbolized as square areas in Fig. 11. From Fig. 11 it can be concluded that nitrification was the main source of N_2O in Exp. 5, which is consistent with the NO_3^- and NH_4^+ distribution in the soil column shown in Fig. 10. Different responses of N_2O emissions from the soil at different water table depths before and after fertilization imply that N_2O production was greatly influenced by the redox potential and by the availability of different N substrates. Our results demonstrate that denitrification dominated N_2O emissions in the unfertilized soil, whereas nitrification was the main source of N_2O production in the fertilized soil. This assumption was supported by the SP values and by the redox potential and N substrate distribution in the soil column.

Implications for Greenhouse Gas Emission Modeling

Modeling GHG emission is essential to regionalize local flux measurements and to develop large-scale GHG budgets (Oertel et al., 2016). Several process-based models have been developed to predict the production, transport, and spatial distribution of GHG in soil (Li et al., 1994; Pattey et al., 2007; Šimůnek and Suarez, 1993). These models have detailed descriptions of the transport processes (e.g., diffusion in liquid and gas phases) and for convection and dispersion in the liquid phase and convection in the gas phase. However, the production of GHG is mostly modeled in a rather simplistic and conceptual way (e.g., using the Michaelis–Menten equation as a control of CO_2 production) (Herbst et al., 2008). In fact, the kinetics of GHG production and consumption control the spatiotemporal variation of GHG, and the lack of representation of important GHG production processes in emission models reduces the applicability of these models across

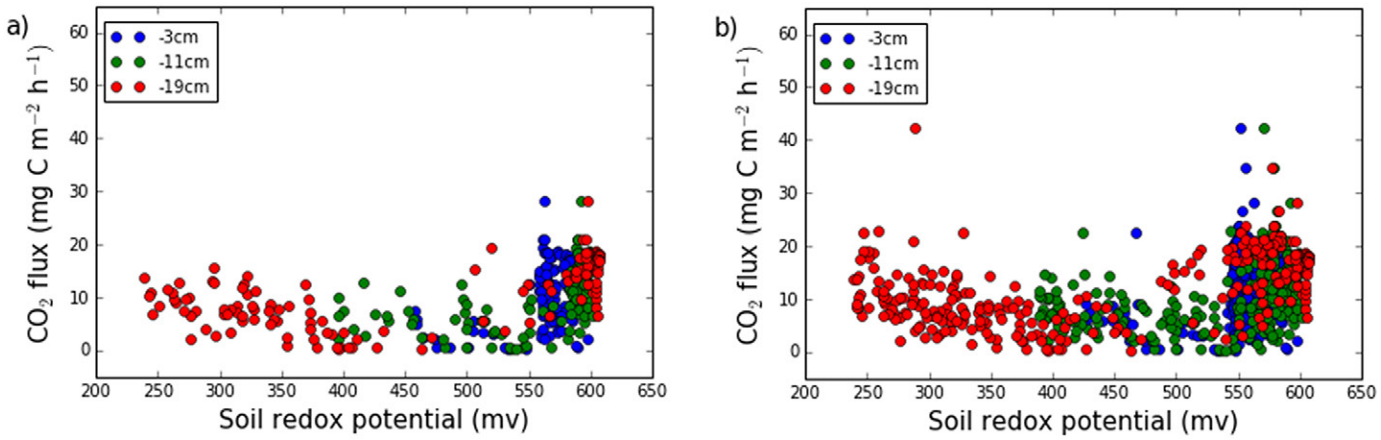

Fig. 8. Carbon dioxide emissions vs. the soil redox potential measured at 3, 11, and 19 cm below the soil surface (a) before and (b) after fertilization.

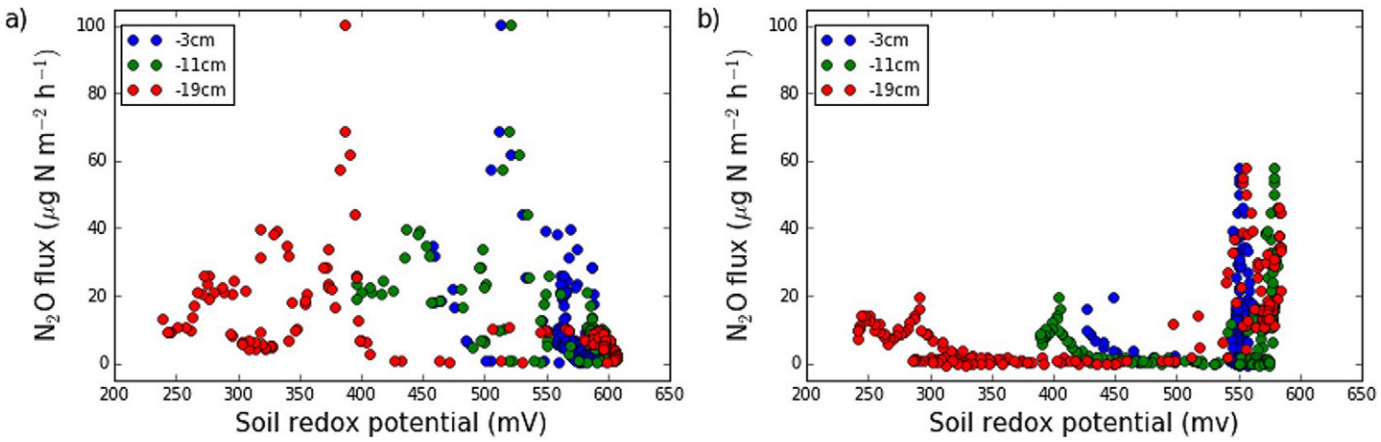

Fig. 9. Nitrous oxide emissions vs. soil redox potential measured at 3, 11, and 19 cm below the soil surface (a) before and (b) after fertilization.

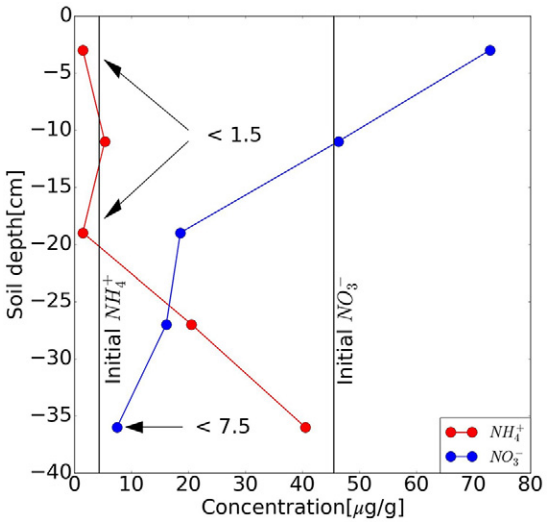

Fig. 10. Concentrations of NH_4^+ and NO_3^- in the lysimeter at the end of Exp. 5 (<1.5 μg g^{-1} for NH_4^+ and <7.5 μg g^{-1} for NO_3^- are the detection limits of the ion chromatography system).

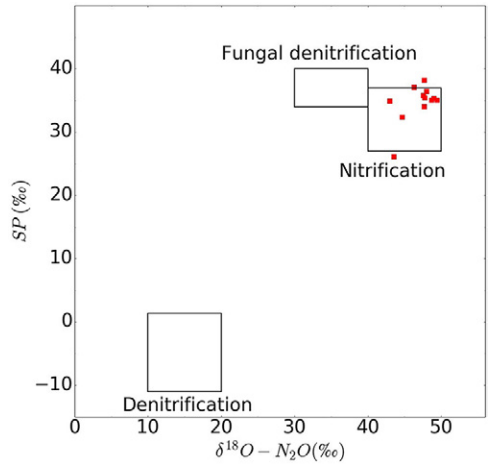

Fig. 11. End-member maps of N_2O source partitioning for Exp. 5. The squares indicate typical ranges for the different processes of N_2O production (Wei et al., 2017); SP, site preference.

different ecosystems (Li et al., 2000). For instance, the simulation of redox potential dynamics in the soil is important to accurately simulate N_2O and NO emission rates because the redox potential determines the dominant production process (e.g., nitrification vs. denitrification). However, most of the GHG models (SoilCO_2, CASA, DNDC, etc.) use soil water content as an indicator of soil aeration status, whereas our results show that the redox potential is often not well correlated with the saturation status (Fig. 4 and 5), which questions the reliability of this simplified approach. A feasible approach would be to incorporate the Nernst equation for redox-active key species in biogeochemical models, such as O_2, NH_4^+, NO_2^-, NO_3^-, NO, and N_2O. In addition, Mn^{4+}/Mn^{2+} and Fe^{3+}/Fe^{2+} should be considered because they have been shown to play an important role in producing N trace gases at specific redox potentials. Thus, in our opinion, measurements of redox potential dynamics would be a better constraint for process-based GHG models, especially related to N_2O and NO. In addition, the redox potential enables the discrimination of the dominant GHG production processes and thus enables a more rigorous testing of new model concepts.

Conclusions

We tested the relationships between changes in soil water potential, soil redox potential, and GHG emissions in laboratory experiments and showed that shifts in soil moisture led to a change in soil redox potential and that those changes in soil redox potential triggered changes in GHG emission flux rates, especially N_2O emissions. Soil redox potential proved to be an important parameter associated with changes in GHG flux rates, and the N_2O flux rate depended also on the availability of NO_3^- and NH_4^+ in the soil. The highest N_2O fluxes occurred at soil redox potentials between 300 and 550 mV before fertilization (indicating denitrification as the main N_2O source process) and >550 mV after fertilization (indicating nitrification as the main N_2O source process). Using an end-member analysis of N_2O isotopic signatures, we were able to confirm this interpretation for one of the experiments. However, our study also had its limitations, such as a lack of replication. Furthermore, in our experiment we applied the fertilizer from the bottom of the soil column, which does not correspond to the common practice of surface application of fertilizers. Because we performed the experiments with only one soil, the applicability of the regression models might be limited to similar soils. Finally, the relationship between redox potential and N_2O emission was found to be discontinuous, preventing the application of simple statistical models. Nevertheless, we could show that redox potential measurements allow the discrimination of the dominant N_2O production processes, enabling a more rigorous testing of GHG models.

Acknowledgments

This work was supported by the Chinese Scholarship Council (Scholarship no. 201506300053) and the TERENO project funded by the Helmholtz Association of German Research Centers. We thank Ansgar Weuthen, Bernd Schilling, Franz Hägel, Franz Leistner, Holger Wissel, Katrin Wagner, and Minghua Zhou for support during the experiments and the two anonymous reviewers for helpful suggestions and comments, which helped to improve the quality of the manuscript.

References

Batjes, N.H. 1996. Total carbon and nitrogen in the soils of the world. Eur. J. Soil Sci. 47:151–163. doi:10.1111/j.1365-2389.1996.tb01386.x

Bhaumik, H.D., and F.E. Clark. 1948. Soil moisture tension and microbiological activity. Soil Sci. Soc. Am. Proc. 12:234–238. doi:10.2136/sssaj1948.03615995001200C0054x

Bogena, H., R. Kunkel, E. Krüger, S. Zacharias, T. Pütz, et al. 2012. TERENO: Long-term monitoring network for terrestrial research. Hydrol. Wasserwirtsch. 56:138–143.

Brettar, I., J.M. Sanchez-Perez, and M. Trémolieres. 2002. Nitrate elimination by denitrification in hardwood forest soils of the Upper Rhine floodplain: Correlation with redox potential and organic matter. Hydrobiologia 469:11–21. doi:10.1023/A:1015527611350

Bruce, J.P., M. Frome, E. Haites, H. Janzen, R. Lal, and K. Paustian. 1999. Carbon sequestration in soils. J. Soil Water Conserv. 54:382–389.

Brümmer, C., N. Brüggemann, K. Butterbach-Bahl, U. Falk, J. Szarzynski, et al. 2008. Soil-atmosphere exchange of N_2O and NO in near-natural savanna and agricultural land in Burkina Faso (W. Africa). Ecosystems

11:582–600. doi:10.1007/s10021-008-9144-1

Butterbach-Bahl, K., E.M. Baggs, M. Dannenmann, R. Kiese, and S. Zechmeister-Boltenstern. 2013. Nitrous oxide emissions from soils: How well do we understand the processes and their controls? Philos. Trans. R. Soc. B 368:20130122. doi:10.1098/rstb.2013.0122

Collier, S.M., M.D. Ruark, L.G. Oates, W.E. Jokela, and C.J. Dell. 2014. Measurement of greenhouse gas flux from agricultural soils using static chambers. J. Vis. Exp. 90:e52110. doi:10.3791/52110

Dalal, R.C., W. Wang, G.P. Robertson, and W.J. Parton. 2003. Nitrous oxide emission from Australian agricultural lands and mitigation options: A review. Soil Res. 41:165–195. doi:10.1071/SR02064

Decock, C., and J. Six. 2013. How reliable is the intramolecular distribution of ^{15}N in N_2O to source partition N_2O emitted from soil? Soil Biol. Biochem. 65:114–127. doi:10.1016/j.soilbio.2013.05.012

Delaune, R.D., and K.R. Reddy. 2005. Redox potential. In: D. Hillel, editor, Encyclopedia of soils in the environment. Vol. 3. Elsevier, Dordrecht, the Netherlands. p. 366–371. doi:10.1016/B0-12-348530-4/00212-5

del Prado, A., P. Merino, J. Estavillo, M. Pinto, and C. González-Murua. 2006. N_2O and NO emissions from different N sources and under a range of soil water contents. Nutr. Cycl. Agroecosyst. 74:229–243. doi:10.1007/s10705-006-9001-6

Fang, C., and J. Moncrieff. 2001. The dependence of soil CO_2 efflux on temperature. Soil Biol. Biochem. 33:155–165. doi:10.1016/S0038-0717(00)00125-5

Farrell, R., G.D.W. Swerhone, and C. van Kessel. 1991. Construction and evaluation of a reference electrode assembly for use in monitoring in situ soil redox potentials. Commun. Soil Sci. Plant Anal. 22:1059–1068. doi:10.1080/00103629109368474

Fiedler, S., M.J. Bepraskas, and J.L. Richardson. 2007. Soil redox potential: Importance, field measurement and observations. Adv. Agron. 94:1–54. doi:10.1016/S0065-2113(06)94001-2

Flessa, H., and F. Beese. 1995. Effects of sugarbeet residues on soil redox potential and nitrous oxide emission. Soil Sci. Soc. Am. J. 59:1044–1051. doi:10.2136/sssaj1995.03615995005900040013x

Gardner, C.M.K., K.B. Laryea, and P.W. Unger. 1999. Soil physical constraints to plant growth and crop production. AGL/MISC/24/99. FAO, Rome.

Heil, J., S. Liu, H. Vereecken, and N. Brüggemann. 2015. Abiotic nitrous oxide production from hydroxylamine in soils and their dependence on soil properties. Soil Biol. Biochem. 84:107–115. doi:10.1016/j.soilbio.2015.02.022

Herbst, M., H.J. Hellebrand, J. Bauer, J.A. Huisman, J. Šimůnek, et al. 2008. Multiyear heterotrophic soil respiration: Evaluation of a coupled CO_2 transport and carbon turnover model. Ecol. Modell. 214:271–283. doi:10.1016/j.ecolmodel.2008.02.007

Hou, A., G. Chen, Z. Wang, O.V. Cleemput, and W. Patrick. 2000. Methane and nitrous oxide emissions from a rice field in relation to soil redox and microbiological processes. Soil Sci. Soc. Am. J. 64:2180–2186. doi:10.2136/sssaj2000.6462180x

Johnson D.W., and P. Henderson. 1995. Effects of forest management and elevated carbon dioxide on soil carbon storage. In: R. Lal et al., editors, Soil management and the greenhouse effects. Lewis Publ., Boca Raton, FL. p. 137–145.

Korres, W., T.G. Reichenau, P. Fiener, C.N. Koyama, H.R. Bogena, et al. 2015. Spatio-temporal soil moisture patterns: A meta-analysis using plot to catchment scale data. J. Hydrol. 520:326–341. doi:10.1016/j.jhydrol.2014.11.042

Kutsch, W.L., M. Bahn, and A. Heinemeyer. 2009. Soil carbon dynamics: An integrated methodology. Cambridge Univ. Press, Cambridge, UK.

Le Mer, J., and P. Roger. 2001. Production, oxidation, emission and consumption of methane by soils: A review. Eur. J. Soil Biol. 37:25–50. doi:10.1016/S1164-5563(01)01067-6

Lewicka-Szczebak, D., J. Augustin, A. Giesemann, and R. Well. 2017. Quantifying N_2O reduction to N_2 based on N_2O isotopocules: Validation with independent methods (helium incubation and ^{15}N gas flux method). Biogeosciences 14:711–732. doi:10.5194/bg-14-711-2017

Li, C., J. Aber, F. Stange, K. Butterbach-Bahl, and H. Papen. 2000. A process-oriented model of N_2O and NO emissions from forest soils: 1. Model development. J. Geophys. Res. 105:4369–4384.

Li, C., S. Frolking, and R. Harriss. 1994. Modeling carbon biogeochemistry in agricultural soils. Global Biogeochem. Cycles 8:237–254. doi:10.1029/94GB00767

Mansfeldt, T. 2004. Redox potential of bulk soil and soil solution concentration of nitrate, manganese, iron, and sulfate in two Gleysols. J. Plant Nutr. Soil Sci. 167:7–16. doi:10.1002/jpln.200321204

Martikainen, P.J., H. Nykanen, P. Crill, and J. Silvola. 1993. Effect of a lowered water table on nitrous oxide fluxes from northern peatlands. Nature 366:51–53. doi:10.1038/366051a0

Masscheleyn, P.H., R.D. DeLaune, and W.H. Patrick. 1993. Methane and nitrous oxide emissions from laboratory measurements of rice soil suspension: Effect of soil oxidation–reduction status. Chemosphere 26:251–260. doi:10.1016/0045-6535(93)90426-6

Mitsch, W.J., and J.G. Gosselink. 2007. Wetlands. 4th ed. John Wiley & Sons, Hoboken, NJ.

Moore, T., and R. Knowles. 1989. The influence of water table levels on methane and carbon dioxide emissions from peatland soils. Can. J. Soil Sci. 69:33–38. doi:10.4141/cjss89-004

Nieder, R., and D.K. Benbi. 2008. Carbon and nitrogen in the terrestrial environment. Springer, Berlin. doi:10.1007/978-1-4020-8433-1

Oertel, C., J. Matschullat, K. Zurba, F. Zimmermann, and S. Erasmi. 2016. Greenhouse gas emissions from soils: A review. Chem. Erde 76:327–352. doi:10.1016/j.chemer.2016.04.002

Olivier, J., and G. Janssens-Maenhout. 2012. CO_2 emissions from fuel combustion. OECD Publ., Paris.

Pachauri, R.K., L. Meyer, G.K. Plattner, and T. Stocker. 2014. Synthesis report. Contribution of Working Groups I, II and III to the Fifth Assessment Report of the Intergovernmental Panel on Climate Change. IPCC, Geneva, Switzerland.

Parkin, T., and R. Venterea. 2010. Chamber-based trace gas flux measurements. In: R.F. Follett, editor, USDA–ARS GRACEnet Project Protocols. USDA–ARS, Washington, DC. p. 3-1–3-39.

Pattey, E., G.C. Edwards, R.L. Desjardins, D.J. Pennock, W. Smith, et al. 2007. Tools for quantifying N_2O emissions from agroecosystems. Agric. For. Meteorol. 142:103–119. doi:10.1016/j.agrformet.2006.05.013

Pezeshki, S., and R. DeLaune. 2012. Soil oxidation-reduction in wetlands and its impact on plant functioning. Biology 1:196–221.

Porter, G., J. Bajita-Locke, N. Hue, and D. Strand. 2004. Manganese solubility and phytotoxicity affected by soil moisture, oxygen levels, and green manure additions. Commun. Soil Sci. Plant Anal. 35:99–116. doi:10.1081/CSS-120027637

Post, W.M., J. Pastor, P.J. Zinke, and A.G. Stangenberger. 1985. Global patterns of soil nitrogen storage. Nature 317:613–616. doi:10.1038/317613a0

Reay, D., E.A. Davidson, K.A. Smith, P. Smith, J.M. Melillo, et al. 2012. Global agriculture and nitrous oxide emissions. Nat. Clim. Change 2:410–416. doi:10.1038/nclimate1458

Rezanezhad, F., R.-M. Couture, R. Kovac, D. O'Connell, and P. Van Cappellen. 2014. Water table fluctuations and soil biogeochemistry: An experimental approach using an automated soil column system. J. Hydrol. 509:245–256. doi:10.1016/j.jhydrol.2013.11.036

Rubol, S., W.L. Silver, and A. Bellin. 2012. Hydrologic control on redox and nitrogen dynamics in a peatland soil. Sci. Total Environ. 432:37–46. doi:10.1016/j.scitotenv.2012.05.073

Ruser, R., H. Flessa, R. Russow, G. Schmidt, F. Buegger, and J. Munch. 2006. Emission of N_2O, N_2 and CO_2 from soil fertilized with nitrate: Effect of compaction, soil moisture and rewetting. Soil Biol. Biochem. 38:263–274. doi:10.1016/j.soilbio.2005.05.005

Sainju, U., J. Jabro, and W. Stevens. 2006. Soil carbon dioxide emission as influenced by irrigation, tillage, cropping system, and nitrogen fertilization. In: V.P. Aneja et al., editors, Workshop on agricultural air quality: State of science, Potomac, MD. 5–8 June 2006. North Carolina State Univ., Raleigh. p. 1086–1098.

Schaufler, G., B. Kitzler, A. Schindlbacher, U. Skiba, M.A. Sutton, and S. Zechmeister-Boltenstern. 2010. Greenhouse gas emissions from European soils under different land use: Effects of soil moisture and temperature. Eur. J. Soil Sci. 61:683–696. doi:10.1111/j.1365-2389.2010.01277.x

Schlesinger, W.H., and J.A. Andrews. 2000. Soil respiration and the global carbon cycle. Biogeochemistry 48:7–20. doi:10.1023/A:1006247623877

Šimůnek, J., and D.L. Suarez. 1993. Modeling of carbon dioxide transport and production in soil: 1. Model development. Water Resour. Res. 29:487–497. doi:10.1029/92WR02225

Smith, K., T. Ball, F. Conen, K. Dobbie, J. Massheder, and A. Rey. 2003. Exchange of greenhouse gases between soil and atmosphere: Interactions of soil physical factors and biological processes. Eur. J. Soil Sci. 54:779–791. doi:10.1046/j.1351-0754.2003.0567.x

Sutka, R.L., G.C. Adams, N.E. Ostrom, and P.H. Ostrom. 2008. Isotopologue fractionation during N_2O production by fungal denitrification. Rapid Commun. Mass Spectrom. 22:3989–3996. doi:10.1002/rcm.3820

Sutka, R.L., N.E. Ostrom, P.H. Ostrom, J.A. Breznak, H. Gandhi, et al. 2006. Distinguishing nitrous oxide production from nitrification and denitrification on the basis of isotopomer abundances. Appl. Environ. Micro-

biol. 72:638–644. doi:10.1128/AEM.72.1.638-644.2006

Tokarz, E., and D. Urban. 2015. Soil redox potential and its impact on microorganisms and plants of wetlands. J. Ecol. Eng. 16:20–30. doi:10.12911/22998993/2801

Toyoda, S., H. Mutobe, H. Yamagishi, N. Yoshida, and Y. Tanji. 2005. Fractionation of N_2O isotopomers during production by denitrifier. Soil Biol. Biochem. 37:1535–1545. doi:10.1016/j.soilbio.2005.01.009

Toyoda, S., N. Yoshida, and K. Koba. 2015. Isotopocule analysis of biologically produced nitrous oxide in various environments. Mass Spectrom. Rev. 36:135–160.

Wang, Z.P., R.D. DeLaune, W.H. Patrick, and P.H. Masscheleyn. 1993. Soil redox and pH effects on methane production in a flooded rice soil. Soil Sci. Soc. Am. J. 57:382–385. doi:10.2136/sssaj1993.03615995005700020016x

Wei, J., W. Amelung, E. Lehndorff, M. Schloter, H. Vereecken, and N. Brüggemann. 2017. N_2O and NO_x emissions by reactions of nitrite with soil organic matter of a Norway spruce forest. Biogeochemistry 132:325–342.

Weigand, H., T. Mansfeldt, R. Baümler, D. Schneckenburger, S. Wessel-Bothe, and C. Marb. 2010. Arsenic release and speciation in a degraded fen as affected by soil redox potential at varied moisture regime. Geoderma 159:371–378. doi:10.1016/j.geoderma.2010.08.014

Weihermüller, L., J. Huisman, A. Graf, M. Herbst, and J.-M. Sequaris. 2009. Multistep outflow experiments to determine soil physical and carbon dioxide production parameters. Vadose Zone J. 8:772–782. doi:10.2136/vzj2008.0041

Wu, D.M., R. Senbayram, N. Well, B. Brüggemann, N. Pfeiffer, et al. 2017. Nitrification inhibitors mitigate N_2O emissions more effectively under straw-induced conditions favoring denitrification. Soil Biol. Biochem. 104:197–207. doi:10.1016/j.soilbio.2016.10.022

Yu, K., F. Böhme, J. Rinklebe, H.U. Neue, and R.D. DeLaune. 2007. Major biogeochemical processes in soils: A microcosm incubation from reducing to oxidizing conditions. Soil Sci. Soc. Am. J. 71:1406–1417. doi:10.2136/sssaj2006.0155

Yu, K., and W.H. Patrick. 2003. Redox range with minimum nitrous oxide and methane production in a rice soil under different pH. Soil Sci. Soc. Am. J. 67:1952–1958. doi:10.2136/sssaj2003.1952

Yu, K., Z. Wang, A. Vermoesen, W.H. Patrick, Jr., and O. Van Cleemput. 2001. Nitrous oxide and methane emissions from different soil suspensions: Effect of soil redox status. Biol. Fertil. Soils 34:25–30. doi:10.1007/s003740100350

Zou, Y., Y. Hirono, Y. Yanai, S. Hattori, S. Toyoda, and N. Yoshida. 2014. Isotopomer analysis of nitrous oxide accumulated in soil cultivated with tea (*Camellia sinensis*) in Shizuoka, central Japan. Soil Biol. Biochem. 77:276–291. doi:10.1016/j.soilbio.2014.06.016